



Published in final edited form as:

Int J Rob Res. 2009 April 1; 28(4): 571–582. doi:10.1177/0278364908100924.

Flagellated Magnetotactic Bacteria as Controlled MRI-trackable Propulsion and Steering Systems for Medical Nanorobots Operating in the Human Microvasculature

Sylvain Martel, Mahmood Mohammadi, Ouajdi Felfoul, Zhao Lu, and Pierre Pouponneau
NanoRobotics Laboratory, Department of Computer and Software Engineering, Institute of Biomedical Engineering, École Polytechnique de Montréal (EPM), Campus of the Université de Montréal, P.O. Box 6079, Station Centre-ville, Montréal (Québec), Canada H3C 3A7

Abstract

Although nanorobots may play critical roles for many applications in the human body such as targeting tumoral lesions for therapeutic purposes, miniaturization of the power source with an effective onboard controllable propulsion and steering system have prevented the implementation of such mobile robots. Here, we show that the flagellated nanomotors combined with the nanometer-sized magnetosomes of a single Magnetotactic Bacterium (MTB) can be used as an effective integrated propulsion and steering system for devices such as nanorobots designed for targeting locations only accessible through the smallest capillaries in humans while being visible for tracking and monitoring purposes using modern medical imaging modalities such as Magnetic Resonance Imaging (MRI). Through directional and magnetic field intensities, the displacement speeds, directions, and behaviors of swarms of these bacterial actuators can be controlled from an external computer.

Keywords

Nanorobots; bacteria; magnetotaxis; medical robotics; bacterial nanorobots; MRI; blood vessels

1. Introduction

A first demonstration of an untethered device propelled and navigated in the blood vessel of a living animal has been recently reported (Martel et al. 2007). In this demonstration being part of a project known as MR-Sub (Magnetic Resonance Submarine), propulsion force was induced on a ferromagnetic core by magnetic gradients produced by the three orthogonal imaging coils of a clinical MRI system. In this type of configuration, external hardware is required to propel untethered objects or nanorobots¹.

To move or actuate untethered devices such as micro- or nanorobots without the need for external hardware dedicated to propulsion, artificial molecular machines built through the assembly of a discrete number of molecular components designed to carry out a specific action jointly have been proposed (Drexler 1992). As such, nanomotors found in nature such as flagellated propulsion mechanisms of bacteria have inspired many researchers trying to mimic them using modern engineering development methods, e.g. (Behkam and Sitti 2005; Behkam

sylvain.martel@polymtl.ca, www.nano.polymtl.ca.

¹Nanorobots are defined here as micro-entities operating under feedback control and relying on parts < 100 nm (approx.) used to implement new embedded functionalities.

and Sitti 2006). A recent example is an artificial flagellum in the form of a nanocoil that has been propelled using a rotating magnetic field (Bell et al. 2007), a technique inspired from a principle theoretically described previously in (Honda et al. 1999). But again, due to technological constraints including but not limited to embedding a power source, this configuration still relies on external hardware for propulsion. So far, nobody has succeeded in developing an autonomous (i.e. without the need for an outside source of power for propulsion) engine capable of sufficient thrust for practical applications.

Instead of developing such autonomous nanomotors, we have proposed another strategy (Martel 2005) which includes the use and integration of bacteria and more specifically Magnetotactic Bacteria (MTB) (Blakemore 1975) with their molecular motors as a means of propulsion or bio-actuation for nanorobots or other micro-scale entities while recognizing their potential for applications in the human blood vessels (Martel 2006). This project dubbed MTBot (*MTB-based robot*) aims at integrating and controlling MTB for developing new generations of nanorobots (bacterial nanorobots) for various applications, a new field of research that could be referred to as bacterial nanorobotics.

The molecular motor embedded in flagellated bacteria measures less than 300 hydrogen atoms across, and has a rotor that can operate at 6,000 to 17,000 revolutions per minute (rpm). With the flagellum acting as a propeller being attached to the rotor, this rotor usually reaches 200 to 1000 rpm. This rotary engine composed of proteins is powered by a flow of protons which makes it particularly attractive in implementations where the availability of electrical power is very limited, as it is often the case for miniature untethered robots.

The validation through experimental data demonstrating the use of a bacterium to push, transport and manipulate a micro-object and the actuation of micro- nanorobots with precise control over the displacement of the bacterium has been first reported in (Martel et al. 2006). This was a significant improvement over the random (uncontrolled) motions of an auto-mobile microchip with bacteria attached previously observed and reported in (Darnton et al. 2004). This demonstration with uncontrolled directional motions was replicated later with chemically stop/resume motion control (Behkem and Sitti 2007) and phototaxis-based stop/resume motion control (Steager et al. 2007)). In the former approach, the introduction of copper ions or ethylenediaminetetraacetic acid in the liquid medium has been proposed. In the latter case, ultraviolet light was used. Although these proposed methods allow the bacterial motion to be stopped or resumed at will, still no directional control was achieved.

More interesting is the fact that our proposed method based on MTB can stop and resume motion at will while controlling the displacement speed from an external computer and without the use of chemical agents, as described in more details later in this paper.

Although nobody has succeeded in controlling the direction of bacteria chemically, there are questions about the viability of using a chemical approach for controlling bacterial actuation for nanorobots. Indeed, there are two major drawbacks in using a chemical approach to control bacterial actuators. First, it is not appropriate for applications in many environments and particularly for operations in the human body. Second, chemical control is not compatible with electronic circuits. This lack of interface with electronics and software-based algorithms/ programs may represent a major obstacle to the implementation of fully controllable nanorobots. As for phototaxis, it is not applicable in many environments including regions deep inside the human body.

On the contrary, the swimming direction of MTB can be controlled by inducing a torque on a chain of nanoparticles called magnetosomes. This torque can be induced from a small directional magnetic field. In turn, this local directional magnetic field can be generated by passing an electrical current through a conductor in the vicinity of the bacteria, hence providing

a suitable, reliable and compatible interface with electrical control/monitoring systems and computers.

2. Controllable Bacterial Actuators

A photograph of a MC-1 MTB is depicted in Fig. 1. Although most people would see it as a simple living organism, in an engineering point-of-view, this bacterium can be considered as a sophisticated actuator with an embedded control interface.

As depicted in Fig. 1, the cell of the MC-1 bacterium is spherical in shape and measures approximately 2 micrometers (μm) in diameter. Each cell has two flagella bundles providing a thrust force exceeding 4 picoNewtons (pN). This value is relatively high compared to other flagellated bacteria with a typical thrust force in the range of 0.3–0.5pN. This allows the MC-1 bacteria to swim in water at room temperature and without load at speeds often exceeding $200\mu\text{m/s}$. This is a very high speed when we know that the swimming speeds of most flagellated bacteria in the same conditions are $\sim 30\mu\text{m/s}$. Maximum displacement speeds of $\sim 300\mu\text{m/s}$ in water at room temperature and corresponding to ~ 150 times its cell's length for a relatively large proportion of the bacteria samples have also been recorded experimentally by our group.

Unlike most bacteria that are based on chemotaxis to detect nutrient gradients and hence influence their motility (Berg and Brown 1972; Ford et al. 1991; Armitage 1992), the direction of displacement of MTB with their chain of magnetosomes which are membrane-based nanoparticles of a magnetic iron, although influenced by chemotaxis and aerotaxis, are also influenced by magnetotaxis (Frankel and Blakemore 1980; Denham et al. 1980; Debarros et al. 1990). But when subjected to a magnetic field slightly higher than the earth's magnetic field of 0.5 Gauss, the directional motions of these MTB become mainly influenced by magnetotaxis and therefore fully controllable by electronics and computers (Martel et al. 2006).

2.1. Choice of MTB

Until now, all MTB that have been studied are motile by means of flagella and as such they could theoretically be considered for the implementation of actuation and propulsion systems for micro- or nanorobots. Practically, although several types of MTB exist and can be found all over the world, the selection process for the type of MTB to be used in robotics is still constrained since only a few types can be cultured in artificial or laboratory conditions.

Most cultured strains belong to the genus *Magnetospirillum* (M.) and include species such as *M. magnetotactium* strain MS-1 (Blackmore et al. 1979), *M. magneticum* strain AMB-1 (Matsunaga et al. 1991), *M. gryphiswaldense* (Schleifer et al. 1991); the marine vibrios strains MV-1 (Bazilinski et al. 1988) and MV-2; a marine coccus, strain MC-1 (DeLong et al. 1993); a marine spirillum, strain MMS-1 (formerly MV-4) (Meldrum et al. 1993); and sulfate-reducing rod-shaped MTB known as *Defulfovibrio magneticus* strain RS-1 (Sakaguchi et al. 1993). But when interfaced to micro- or nanorobots, higher swimming speeds typically become one of the key factors for selecting the right MTB. In general, the magnetotactic spirilla are at the slower end ($<100\mu\text{m/s}$) while the magnetotactic cocci are at the faster end at $>100\mu\text{m/s}$. As such, strain of MC-1 cells² seems to be a good choice and has been selected in this particular study (peak speeds approaching $300\mu\text{m/s}$ have been measured experimentally by our group as stated earlier). If the size of the MTB is an important aspect to consider, the MV-4 bacterium is the smallest with a length of $\sim 0.5\mu\text{m}$ compared to $\sim 2\mu\text{m}$ for the MC-1 but the choice for a smaller cell is done at the cost of slower swimming speeds (range of $\sim 30\text{--}80\mu\text{m/s}$). Both previous types have two bundles of flagella on one side of the cell and they are classified as polar MTB. Polar

²The MC-1 bacteria used in this study were cultivated at the NanoRobotics Laboratory at EPM in incubators using special controlled procedures and environmental conditions.

MTB swim persistently in one direction along the magnetic field. Polar MTB unlike axial MTB are generally more suitable for controlled untethered devices such as nanorobots since they are usually more predictable when controlling their swimming directions. For instance, some cells have two FBs on both ends. These MTB swim in both directions along the magnetic field lines with frequent reversals of swimming directions with approximately the same number of bacteria swimming in each direction. Because of this behaviour, they are classified as axial MTB. The *Magnetospirillum gryphiswaldense* bacterium is one example with a length varying between $\sim 1\text{--}3\mu\text{m}$, a width of $\sim 0.5\mu\text{m}$ and swimming speeds in the range of $\sim 40\text{--}80\mu\text{m/s}$.

3. Propulsion and Terminal Velocity

The shape of the bacterial flagellum acting like a propeller consists of a 20 nanometer (nm) - thick hollow tube. It has a helical shape with a sharp bend outside and next to the outer membrane. Put together, they form what looks like a hook where a shaft runs between the hook and the basal body. The shaft then passes through protein rings in the cell's membrane that act as bearings. Counter-clockwise rotations of a polar flagellum thrust the cell forward.

For propulsion or transport purpose, the thrust force provided by each MTB is the key factor to consider in the evaluation of the terminal velocity. The terminal velocity v_T of a single MC-1 MTB can then be estimated (discounting the effect of the trailing flagella and assuming a constant rotational speed of the flagellum or a constant protons flux in the molecular motor) from Stokes' equation as

$$v_T = \frac{F_T}{3\pi\eta d}, \quad (1)$$

where in our particular case subjected to our experimental and cultivation conditions, $4.7 \times 10^{-12} \geq F_T \geq 4.0 \times 10^{-12}$ N with $\eta = 1.0 \text{mPa}\cdot\text{s}$ in water at 20°C represent the thrust force and the viscosity of the medium respectively, while $d \approx 2 \times 10^{-6}$ m represents the diameter of the cell when unloaded. Notice that the diameter of the entire moving body could increase when loaded.

Similar to tolerances for mechanical or electrical parts, the engineers must cope with tolerances in terminal velocities for MTB and as for engineered parts, a preselection will be essential if precise specifications are required in the implementation. The initial swimming speed distribution of unloaded and unselected (i.e. without a priori selection processes) MC-1 MTB in an aqueous medium at room temperature is depicted in Fig. 2.

The swimming speeds from a significantly large sample of MC-1 MTB have been measured in our laboratory with a video camera AxioCam MRm from Carl Zeiss mounted on an optical microscope (Zeiss Axio-Imager) using the following settings: Magnetic field of 20 Gauss, objective Long Distance (LD) Epiplan 20 \times , in reflection-mode microscopy using dark-field illumination.

3.1 Effect of Body Temperature on the Terminal Velocity

Our experimental results show that an increase of the temperature level T will influence the terminal velocity of MC-1 MTB. When MC-1 MTB are considered for medical nanorobots designed for operations in the human body where $T = 37^\circ\text{C}$, the experimental results as depicted in Fig. 3 show that the terminal velocity of MC-1 MTB will decay for a duration of ~ 40 minutes. Although the viscosity of blood at such a temperature is $3\text{--}4 \text{mPa}\cdot\text{s}$, considering that the cell's

size of the MC-1 MTB is smaller than a single red cell, the viscosity of plasma which is approximately equivalent to water has been considered.

3.2 Loading MTB while Maintaining Maximum Velocity

In this particular context, MTB can be used to propel a load which may take various forms such as nano- or microparticles carrying therapeutic agents or acting as biosensors, to larger objects typically capable of more sophisticated functions for the implementation of a more technologically advanced nanorobot, e.g. (André and Martel 2006). Figure 4 shows four loading strategies where MTB can be used for propulsion.

Although several loading strategies can be applied, for operations such as the delivery of therapeutic agents to a tumoral lesion requiring transitions through capillary sections of the human microvasculature, the method showed in Fig. 4a and Fig. 4b become quite attractive. The method depicted in Fig. 4a was validated by our group in an experiment that aimed at loading fluorescent cell penetrating peptides (FITC-LC-Antennapedia – Anaspec, San Jose, CA 95131) inside the MC-1 cell. Although promising, more work need to be done before it becomes an effective means of delivery for such applications. Nonetheless, this approach still considered for future improvement as a targeting of cytotoxic agents or radio-active substances.

For many target delivery applications in the microvasculature, the method depicted in Fig. 4b is quite attractive. Here, biodegradable polymeric nanoparticles for instance with an overall diameter of ~150 nm can be attached to the MTB-cell. The use of antibodies³ is one practical and efficient method to attach such nanoparticles in this particular case. The size of the nanoparticles is chosen large enough to contain sufficient therapeutic agent while being small enough not to add significant drag force to the cell.

3.3 Capillary Wall Effect on Bacterial Nanorobots

According to Stokes' law, the drag force D in low Reynolds number ($Re < 1$) hydrodynamics as encountered in the human microvasculature can be derived from Eq. 1 and computed as

$$D=3\pi\eta dv_T; \quad 0 \leq Re \leq 1. \quad (2)$$

Such opposing drag force is then proportional to the viscosity of the medium, the diameter of the moving object, here considering the cell's size combined with the load, and the velocity of the object (Kundu and Cohen, 2002), here being the bacterial carrier or nanorobot without noticeable effect from the shape of the object itself.

Although the size or diameter of each bacterial carrier or nanorobot could theoretically be increased with additional loads hence increasing drag force, other factors influencing the speed of the MTB in the particular environment where they operate must also be taken into account. For instance, when moving or navigating in smaller capillaries, the drag force acting against the spherical MC-1 cell is a function of $\lambda = d/d_C$ which is the ratio between d as defined earlier and the diameter of the capillary d_C , a phenomenon also known to as the wall retardation effect (Fidleris and Whitmore, 1961). When the diameter ratio approaches unity, the wall effect becomes predominant. In the worst case, we expect a $min d_C \approx 4$ to 5×10^{-6} m for the small capillaries in human including blood vessels created by angiogenesis, i.e. vessels used prior to reach the tumoral regions for applications such as target chemotherapies for instance. Hence a worst case $\lambda \approx 0.5$ or slightly higher if nanoparticles are loaded would be expected as a

³These antibodies specific to the MC-1 cells have already been developed and tested successfully at the NanoRobotics Laboratory at EPM.

maximum ratio for the MC-1 bacterial nanorobots. From classical theory, the wall effect on the velocity of the bacteria v can be estimated (Francis 1933; Fidleris and Whitmore 1961) as

$$\frac{v}{v_{\infty}} = \left(\frac{1 - \lambda}{1 - 0.475\lambda} \right)^4 \quad (3)$$

where v_{∞} is the velocity of the bacteria in open space. With $v_{\infty} = 256.25 \mu\text{m/s}$ (global value estimated from experimental data, see Fig. 2), the swimming speed of the bacteria should decrease from $256.25 \mu\text{m/s}$ down to $48.38 \mu\text{m/s}$. It is interesting to note that our preliminary experimental data depicted in Fig. 5 show that the MC-1 cells swim much faster in a narrow channel when submitted to the wall effect than the speed predicted using Eq. 3. Indeed, although the theoretical estimation predicts that the swimming speed should decrease by approximately 81% (from $256.25 \mu\text{m/s}$ down to $48.38 \mu\text{m/s}$) when the width of the channel shrinks from $12 \mu\text{m}$ to $4 \mu\text{m}$.

The data in Fig. 5 were recorded with a group of 30 bacteria under a directional field of 20 Gauss at constant environmental conditions and at room temperature. The bacteria were taken from a fresh culture. The data recorded under optical microscopy show that compared to a microbead of the same size and submitted to the same force observed from the MC-1 cells in open space, that the bacteria still swim faster in smaller diameter channels.

The results presented in Fig. 5 are in accordance with similar observations done in a previous study (Mitchell et al. 1995). This may suggest, although more experiments are needed, that the thrust force of bacteria could increase significantly to compensate for attenuating forces such as the wall effect.

In other words, it may be possible although it is too early to confirm it that the MC-1 cell may compensate such opposing force by increasing the protons flux in order to increase the rotational rate of the flagella. But this assumption needs further investigations. But if this is the case, there will be a maximum limit in the flow of protons and such additional compensation may end up being non significant in this particular case. Nonetheless, such additional protons flux which has been recorded in previous experiments under certain conditions is most likely to shorten the lifespan of the bacteria when no nutrients are available. Hence, considering the relatively short lifespan of the MC-1 MTB in more severe conditions such as the one plotted in Fig. 3, this may not be suitable in this particular context.

It is then interesting to notice that since $d \approx 2\mu\text{m}$ for the MC-1 bacterium, we will have an ideal worst case $\lambda \approx 0.5$ in the smallest capillaries, while providing some room to attach nanoparticles at the surface of the cell without increasing significantly wall retardation effect.

3.4 Controlling the Velocity of Bacterial Nanorobots

As depicted in Fig. 1 and mentioned earlier, each MTB synthesizes in their cell a chain of membrane-based nanoparticles called magnetosomes. Besides being used for controlling their swimming directions, these magnetosomes can also be used to control their swimming speeds with any values between and including zero and their maximum swimming speeds. This is shown in Fig. 6.

The results plotted in Fig. 6 show also that not only genetic modifications but the conditions of culture alone can be used to adjust the characteristics of the MTB. A DC magnetic field allows us to control the velocity of bacterial nanorobots while offering an interface with electrical computing systems without the use of chemical agents. Although the DC magnetic

field is not required to achieve maximum velocities which is a really positive feature in other applications relying on bacterial nanorobots, reducing or even stopping the movement of bacterial nanorobots may be highly suitable in some particular applications including but not limited to direct medical targeting interventions inside the human body. For instance, for navigating nanorobots directly towards a pre-defined target inside the human body, a guiding system must be implemented. Without such guiding system, such nanorobots would get lost in the maze that represents the human vascular network which is constituted of close to 100,000 km of blood vessels.

As depicted in Fig. 6, to stop a single or an entire swarm of bacterial nanorobots without chemical agents, a DC magnetic field with sufficient magnitude must then be applied. Although further investigations need to be done, the experimental results plotted in Fig. 6 suggest that the 1.5 T or higher DC magnetic fields typically found in the bore of modern clinical MRI systems would stop the swimming movement of such bacterial nanorobots, allowing easier and more accurate determination of their position in the human body. Controlled speeds of the bacterial nanorobots can then be resumed in a special configuration as discussed later in this paper.

4. Tracking MTB-based Nanorobots with MRI

As mentioned earlier, being able to track such medical nanorobots inside the human body is essential for applications involving direct targeting. The magnetosomes embedded in each MC-1 MTB as shown in Fig. 7 are Fe₃O₄ single magnetic domain crystals of a few tens of nanometers in size. Similar to nanoparticles used for MRI contrast agents, magnetosomes cause a local distortion of the magnetic field inside the bore of a clinical MRI system. The local magnetic field distortion from each magnetosome can be approximated at a point P of coordinate $r(x, y, z)$ by that of a magnetic dipole as described by Eq. 4 as

$$\vec{B}(P) = \frac{\mu_0}{4\pi} \left(3 \frac{(\vec{m} \cdot \vec{r}) \vec{r}}{r^5} - \frac{\vec{m}}{r^3} \right), \quad (4)$$

where $\mu_0 = 4\pi 10^{-7} \text{ H}\cdot\text{m}^{-1}$ is the permeability of free space. For a uniformly magnetized object, the dipolar magnetic moment ($\text{A}\cdot\text{m}^2$) is given by

$$\vec{m} = \frac{4}{3} \pi a^3 \vec{M}_{SAT} \quad (5)$$

where \vec{M}_{SAT} is the saturation magnetization of the object, and a its radius (m) considering a spherical shape. A numerical simulation of a single bacterium magnetic field plotted over an electron microscopy image is depicted in Fig. 7. The simulation results assume 11 aligned magnetosomes, each with a diameter of 70nm. The magnetosome chain significantly disturbs the local magnetic field.

As depicted in Fig. 8a, the field perturbation is significant near the bacterium with values greater than 100 ppm and decreases further away from the bacterium. This is quite significant for our application considering that an accepted homogeneity level of modern MRI clinical scanner is approximately 5 ppm over a 50 cm diameter spherical volume at 1.5 T. These perturbations mostly affect the spin-spin (T₂) relaxation times as depicted in Fig. 8b, where several concentrations of MTB were imaged using a fast spin echo sequence. These results suggest that MRI could potentially be used to track MTB in 3D inside the human body providing a

superior imaging modality compared to existing medical imaging methods for this particular application. These images were run with a Siemens Avanto 1.5T clinical scanner using a wrist antenna. The sequence parameters were: TR/TE = 5620/127ms, slice thickness of 20 mm, and pixel spacing of 0.254 mm.

5. Steering Control

A magnetic field will exert a torque on a ferromagnetic material such as magnetite or on a material with diamagnetic anisotropy. Only ferromagnetic or superparamagnetic crystals with length below 35 nm are able to produce a response to a field as weak as the geomagnetic field (0.5 Gauss) that is detectable against thermal motion. Magnetosomes within the permanent single domain size range are uniformly magnetized providing the maximum magnetic dipole moment per unit volume. When arranged in a chain as it is the case for the MC-1 MTB, magnetostatic interactions between the single domain crystals cause the magnetic moments to spontaneously orient parallel to each other along the direction of the chain resulting in a permanent magnetic dipole for the entire chain with a magnetization approaching its saturation value at 0.6T. Hence, the magnetite chain in magnetotactic bacteria acting like a compass needle can be rotated by a magnetic field because of the torque exerted on their magnetite particles. In other words, this chain of magnetosomes imparts to the MTB a magnetic moment that generates sufficient torque so that the bacteria can align themselves to magnetic field lines. This is referred to as magnetotaxis. Some examples performed by our group of computer-based directional control based on magnetotaxis of MTB recorded using optical microscopy are depicted in Fig. 9.

The swimming direction of MTB is influenced not only by magnetotaxis but also by aerotaxis and chemotaxis. Aerotaxis is defined as the movement of an organism, especially a bacterium, toward or away from air or oxygen while chemotaxis is defined as directed movement of a cell or organism toward (or away from) a chemical source. Although at lower magnetic field intensities, i.e. around the geomagnetic field of 0.5 Gauss, magnetotaxis has an influence on the swimming directions of MTB, previous experiments conducted by our group show that a higher magnetic field with a minimum value of approximately 3 Gauss (or even less) provides the best control and responses of the MTB from directional commands generated by an electrical source by making magnetotaxis the predominant factor over chemotaxis and aerotaxis.

With regards to thermal noises, it has been reported and estimated that the magnetic moment for the smaller organisms are $1.0 \times 10^{-15} \text{Am}^2$, with a corresponding magnetic energy in the geomagnetic field of $50 \mu\text{T}$ is $5.0 \times 10^{-20} \text{J}$. This value is already $\sim 10 \times$ the thermal energy at room temperature. Hence, in a controlled environment (where the effects of aerotaxis and chemotaxis are negligible), the average orientation of the cell along the magnetic field as it swims is determined by the ratio of magnetic to thermal energy. Hence for a ratio of 10, the average projection of the magnetic dipole on the magnetic field is 0.9 meaning that the MTB will migrate along the field at 90% of its forward speed. Hence, by increasing the intensity of the directional field up to a certain limit, more accurate directional control can be achieved.

In some instances, the combination of sensory information such as chemotaxis or aerotaxis with magnetotaxis to influence the motion of the MTB-based nanorobots may be suitable. For instance, polar magneto-aerotaxis keeps cells at the preferred oxygen concentration at the oxic-anoxic interface. This feature could potentially be integrated at a specific moment in the control protocol to enhance tumour targeting where a decrease in the concentration oxygen exists.

6. Effect of Vessel Geometries

When a swarm of MTB or bacterial nanorobots move in a given direction (see video extension 1) to deliver sufficient therapeutic compounds to a tumor for instance, dispersion or loss in density of the agglomeration due to swimming speed variation among the MTB and inter-MTB interactions may occur over a relative short time. Over time, such dispersion could reduce local field perturbations below a minimum threshold required for the swarm to be detectable inside the human body depending on the limit in sensibility of the detection system and the imaging modality being used. Fortunately, the complex vessel network geometry can be exploited to maintain grouping through successive small displacement segments.

7. Coercivity-based Control

In our particular context, coercivity H_C is defined as the minimum field strength required for flipping the magnetic moment of a uniform magnetized (single domain) crystal from one stable direction to another. Hence, such coercivity could potentially be considered in the navigation protocol of the bacterial nanorobots to enhance targeting effectiveness in the human body. For instance, it has been reported that a magnetic pulse of higher intensity than H_C induce a complete reversal of the magnetotactic direction (Kalmijn and Blakemore 1978) without affecting the viability of the cells (Hedges 1985), a technique referred to as pulse re-magnetization. For MTB, we expect $H_C \approx 30\text{mT}$ (300 Gauss) as reported in (Blakemore et al. 1985; Mann et al. 1987) for instance. This value can be increased up to an H_C^{max} which can be approximately twice the original H_C using a pulse magnetization technique (Diaz Ricci et al. 1991).

The effect of a pulse re-polarization on the percentage of re-polarized MC-1 cells from experimental data obtained by our group is depicted in Fig. 10. Once re-polarized (re-magnetized), the bacteria will continue swimming in the same original direction until they reach an obstacle. When reaching an obstacle, the MTB will begin swimming in the reverse direction if re-polarized. Prior to reach an obstacle, the MTB swimming speed is reduced according to the magnitude of the pulse and will resume the initial speed after the pulse.

Moreover, our group also observed that using a magnetic field with a magnitude of at least ~ 120 Gauss that the MTB will swim in the reverse direction when encountering an obstacle (with a sufficiently large surface), otherwise the MTB will continue swimming persistently towards the obstacle. This feature is presently considered as an enhancement to the navigation/control algorithm for increasing targeting effectiveness for bacterial nanorobots operating in the angiogenesis network.

8. Biocompatibility

For nanorobots operating in the blood vessels, biocompatibility is an important issue to consider. The degradation products of the non-pathogenic bacteria can have a cytotoxic effect at relatively high concentration. Under $80\mu\text{l}$ of bacteria solution (density of 5×10^4 cells/ $200\mu\text{l}$ in cell culture solution) in a $200\mu\text{l}$ well, our preliminary tests showed that the cell viability is higher than 90%. The cell viability is increasing with exposure time which indicates the non-cytotoxic effect of the bacteria at this volume. This cell viability assay also shows that the bacteria biocompatibility depends on the bacteria volume, hence imposing a limit on the quantity of bacterial nanorobots that can be presented in the body at any given time. Therefore, the number of bacterial nanorobots used should be high enough to deliver a sufficient amount of therapeutic agents with a density sufficient to be MR-trackable while being lower than the cytotoxicity limit. Nonetheless, this issue needs further studies with bacteria degradation products analysis and haemocompatibility assays as platelet adhesion, leukocytes activation

and haemolysis assay. The results of these assays will give further insight through experimental data on the bacteria concentration which can be used safely for *in vivo* assays.

9. Targeting Strategy

As in a naval force where a fleet of various types of combat platforms can provide more effective strategies against the enemy, several types of medical nanorobots may prove to be more effective for fighting tumours. For instance, slightly larger “embolization nanorobots” can be used to temporarily reduce blood flow in capillaries and hence facilitating the steering of “targeting nanorobots” towards a tumour. Small diameter blood vessels are presently not visible on any medical imaging systems preventing effective path planning to reach the target. Hence, “scout nanorobots” acting as navigable MRI contrast agents can also be used to gather information that will be used to plan the final attack.

Figure 11 shows that bacterial nanorobots propelled by a single MC-1 cell may be advantageous over the induction of force on a ferromagnetic material for navigation in the blood vessels as demonstrated *in vivo* in (Martel et al. 2007) for devices smaller than $\sim 2\text{--}3\mu\text{m}$ in diameter. As the total volume dedicated to the ferromagnetic or superparamagnetic nanoparticles decreases, the total induced propulsion force is also reduced significantly.

Although blood flow velocities are lower in smaller diameter blood vessels compared to larger ones, additional magnetic gradient coils inside the MRI system must still be considered. But as the magnetic gradients increase to compensate for smaller volumes of ferromagnetic materials, the coils begin to overheat. Hence, to prevent a shut-down of the system which may result to tragic consequences for the patient, the time dedicated to propulsion and steering of the nanorobots must be decreased during the tracking/propulsion cycles to allow time for the coils to cool down. The limited time dedicated to steering or propulsion may impact in some situations targeting effectiveness. Even by using the best ferromagnetic materials available such as Iron-Cobalt for inducing the maximum force per volume unit, this still may remain an issue when navigating in the microvasculature. This limitation is getting even worse when proven biocompatible materials but offering less propulsion power density such as Iron-Oxide is considered to avoid additional design complexities intended to prevent toxic Cobalt ions to come in direct contact with blood. As such, the molecular motor of the MC-1 bacterium can become very useful when operating in the microvasculature.

Similarly, although efficient in the microvasculature, the thrust force of MTB is insufficient to cope with the higher flow rates typically encountered in larger blood vessels. This may suggest the need for ferromagnetic carriers propelled and steered using magnetic gradients and designed to encapsulate and carry bacterial nanorobots passed the arterioles, and ideally at the entrance of the capillary network. This is represented schematically in Fig. 12. Pre-synthesized biodegradable polymer or hyperthermia-based techniques used to elevate the temperature of embedded nanoparticles could be used as release methods. The same carrier could be used for temporary embolization (where the name embolization carrier in Fig. 12) to facilitate targeting with MTB-based nanorobots.

10. Robotic Platform

A basic diagram of a MRI-based robotic platform adapted for ferromagnetic and bacterial nanorobots is depicted in Fig. 13. Although such platform relies on several software modules and algorithms, only the main hardware components are shown for simplicity.

A conventional clinical MRI system is upgraded with additional coils represented in bold in Fig. 13 with their respective Amplifiers Unit (AU). Although the encoding gradients coils are sufficient to propel larger ferromagnetic carriers or robots in the blood vessels, the additional

3D Steering Gradients Coils (SGC) are required to steer smaller ferromagnetic or superparamagnetic carriers or robots. Although other medical imaging platforms could be upgraded for navigating bacterial nanorobots and be implemented with much less complexity than with MRI, the use of MRI provides many advantages that may be worth the additional implementation and control complexity such as the possibility for three-dimensional imaging inside the human body, enhanced tissue contrast, lack of radiation, the presence of a large homogeneous magnetic field inside the bore of the MRI system which is sufficient to bring the magnetic material of the ferromagnetic robots to saturation, and the availability of MRI systems in clinics and hospitals making technology transfers and acceptance easier while reducing the cost of implementing the technology.

As depicted in Fig. 13, the use of bacterial nanorobots require the addition of 3D Steering Magnetic Coils (SMC) located just outside of the entrance of the MRI bore, at a location where the DC magnetic field of the MRI system is negligible and where a torque can be induced on the chain of magnetosomes embedded in the MTB. The entry/exit process provided by the mechanical table is taking into account in the control algorithms.

11. Summary and Conclusion

The real challenge in the development of medical micro-nanorobots designed to operate in the human blood vessels goes behind the aspect of propulsion alone. In this paper, we show that a fully operational robotic platform must address the integration of many inter-disciplinary components and methods within tight real-time, technological and physiological constraints. We also concluded that most likely, various types of nanorobots with different dimensions and characteristics will also be required to navigate effectively in the complex network comprised of various diameter blood vessels and flow rates. This will prove to be more important as we attend to enhance targeting effectiveness in the microvasculature when such nanorobots will need to transit through larger diameter vessels in the human blood network. Through experimental results and theoretical formulations, we also showed the advantages of integrating biological components and more specifically Magnetotactic Bacteria (MTB) for the development of hybrid (made of synthetic and biological components) nanorobots adapted to operate in the human microvasculature. We also showed methods of directional and velocity controls and demonstrated that **the** some behaviours and characteristics of the MTB can be altered. More important is the fact that all these methods can be controlled from an electronic system. Finally, an imaging modality to track the bacterial nanorobots have been proposed and validated with a clinical MRI system, allowing closed-loop navigation control of the medical nanorobots by computer towards specific destinations in the human body.

Supplementary Material

Refer to Web version on PubMed Central for supplementary material.

Acknowledgments

We acknowledge the help of Prof. Yahye Merhi from the Montréal Heart Institute for his help in the realization of the biocompatibility assays. This project is supported in part by the Canada Research Chair (CRC) in Micro/Nanosystem Development, Fabrication and Validation and grants from the National Sciences and Engineering Research Council of Canada (NSERC), the Province of Québec, and the Canada Foundation for Innovation (CFI). This project is also supported in part by US Grant Number R21EB007506 from the National Institute Of Biomedical Imaging And Bioengineering. The content is solely the responsibility of the authors and does not necessary represent the official views of the National Institute Of Biomedical Imaging And Bioengineering or the National Institutes of Health.

References

- André, W.; Martel, S. Initial design of a bacterial actuated microrobot for operations in an aqueous medium. Proc. of the 28th IEEE-EMBS Annual Int. Conf. of the Eng. in Med. and Biol. Soc. (EMBS); 2006. p. 2824-2827.
- Armitage JP. Bacterial motility and chemotaxis. Sci Progr 1992;76:451-477.
- Bazylinski DA, Frankel RB, Jannasch HW. Anaerobic magnetite production by a marine, magnetotactic bacterium. Nature 1988;334:518-519.
- Behkam, B.; Sitti, M. Modeling and testing of a biomimetic flagellar propulsion method for microscale biomedical swimming robots. Proc. of the 2005 IEEE/ASME Int. Conf. on Advanced Intelligent Mechatronics (AIM 2005); 2005. p. 37-42.
- Behkam B, Sitti M. Design methodology for biomimetic propulsion of miniature swimming robots. Journal of Dynamic Systems, Measurement and Control, Trans of the ASME 2006;128(1):36-43.
- Behkam B, Sitti M. Bacterial flagella-based propulsion and on/off motion control of microscale objects. Appl Phys Lett 2007;90:023902-4.
- Bell, DJ.; Leutenegger, S.; Hammar, KM.; Dong, LX.; Nelson, BJ. Flagella-like propulsion for microrobots using a nanocoil and a rotating electromagnetic field. Proc. of the 2007 IEEE Int. Conf. on Robotics and Automation (ICRA 2007); 2007. p. 1128-1133.
- Berg HC, Brown DA. Chemotaxis in *Escherichia coli* analyzed by three-dimensional tracking. Nature 1972;239:500-504. [PubMed: 4563019]
- Blakemore RP. Magnetotactic bacteria. Science 1975;190:377-379. [PubMed: 170679]
- Blakemore RP, Maratea D, Wolfe RS. Isolation and pure culture of a freshwater magnetic spirillum in chemically defined medium. J Bacteriol 1979;140:720-729. [PubMed: 500569]
- Blakemore RP, Short KA, Bazylinski DA, Rosenblatt C, rankle RB. Microaerobic conditions are required for magnetite formation within *Aquaspirillum magnetotacticum*. Geomicrobiol J 1985;4:53-71.
- Darnton N, Turner L, Breuer K, Berg HC. Moving fluid with bacterial carpet. Biophys J 2004;86:1863-1870. [PubMed: 14990512]
- Debarros H, Esquivel DMS, Farina M. Magnetotaxis. Sci Progr 1990;74:347-359.
- Delong EF, Frankel RB, Bazylinski DA. Multiple evolutionary origins of magnetotaxis in bacteria. Science 1993;259:803-806. [PubMed: 17809345]
- Denham C, Blakemore R, Frankel R. Bulk magnetic properties of magnetotactic bacteria. IEEE Trans on Magnetism 1980;16(5):1006-1007.
- Diaz Ricci JC, Woodford BJ, Kirschvink JL, Hoffmann MR. Alteration of the magnetic properties of *Aquaspirillum magnetotacticum* by pulse magnetization technique. Appl and Env Microb 1991;57(11):3248-3254.
- Drexler, KE. Nanosystems: molecular machinery, manufacturing, and computation. John Wiley and Sons; New York, USA: 1992.
- Fidleris V, Whitmore RL. Experimental determination of the wall effect for spheres falling axially in cylinder vessels. Br J Appl Phys 1961;12:490-494.
- Francis AW. Wall effect in falling ball method for viscosity. Physics 1933;4:403-406.
- Frankel RB, Blakemore RP. Navigational compass in magnetic bacteria. J of Magn and Magn Materials 1980;15-18(3):1562-1564.
- Ford RM, Phillips BR, Quinn JA, Lauffenburger DA. Measurement of bacterial random motility and chemotaxis coefficients. I. Stopped-flow diffusion chamber assay. Biotech and Bioeng 1991;37(7):647-660.
- Hedges RW. Inheritance of magnetosome polarity in magnetotactic bacteria. J Theor Biol 1985;112:607-608.
- Honda T, Arai K, Ishiyama K. Effect on micro machine shape on swimming properties of the spiral-type magnetic micro-machine. IEEE Trans on Magnetics 1999;35:3688-3690.
- Kalmijn, AJ.; Blakemore, RP. The magnetic behavior of mud bacteria. In: Schmidt-König, K.; Keeton, WT., editors. Proceedings in life science. Animal migration, navigation and homing; Berlin: Springer-Verlag KG; 1978.
- Kundu, P.; Cohen, I. Fluid Mechanics. Vol. 2. Academic; 2002.

- Mann, S.; Sparks, NHC.; Blakemore, RP. Ultrastructure and characterization of anisotropic magnetic inclusions in magnetotactic bacteria. *Proc. R. Soc. Lond. B*; 1987. p. 469-476.
- Martel, S. Method and system for controlling micro-objects or micro-particles. US Pat Appl. 11/145,007. 2005.
- Martel, S. Targeted delivery of therapeutic agents with controlled bacterial carriers in the human blood vessels. 2nd ASM/IEEE EMBS Conf. on Bio, Micro and Nanosystems; San Francisco, USA. 2006.
- Martel S, Tremblay C, Ngakeng S, Langlois G. Controlled manipulation and actuation of micro-objects with magnetotactic bacteria. *Appl Phys Lett* 2006;89:233804–6.
- Martel S, Mathieu J-B, Felfoul O, Chanu A, Aboussouan É, Tamaz S, Pouponneau P, Beaudoin G, Soulez G, Yahia L'H, Mankiewicz M. Automatic navigation of an untethered device in the artery of a living animal using a conventional clinical magnetic resonance imaging system. *Appl Phys Lett* 2007;90:114105–7.
- Matsunaga T, Sakaguchi Y, Tadokoro F. Magnetite formation by a magnetic bacterium capable of growing aerobically. *Appl Microbiol Biotechnol* 1991;35:651–655.
- Meldrum FC, Mann S, Heywood BR, Frankel RB, Bazylinski DA. Electron microscope study of magnetosomes in two cultured vibrioid magnetotactic bacteria. *Proc Roy Soc Lond B* 1993;251:237–242.
- Mitchell JG, Pearson L, Dillon S, Kantalis K. Natural assemblages of marine bacteria exhibiting high-speed motility and large accelerations. *Appl and Env Microbiol* 1995;61(12):4436–4440. [PubMed: 8534107]
- Sakaguchi T, Burgess JG, Matunaga T. Magnetite formation by a sulphate reducing bacterium. *Nature* 1993;365:47–49.
- Schleifer K-F, Shüler D, Spring S, Weizenegger M, Amann R, Ludwig W, Kohler M. The genus *Magnetospirillum* gen. nov., description of *Magnetospirillum gryphiswaldense* sp. nov. And transfer of *Aquaspirillum magnetotacticum* to *Magnetospirillum magnetotacticum* comb. nov. *Syst Appl Microbiol* 1991;14:379–385.
- Steager E, Kim C-B, Patel J, Bith S, Naik C, Reber L, Kim MJ. Control of microfabricated structures powered by flagellated bacteria using phototaxis. *Appl Phys Lett* 2007;90:263901–3.

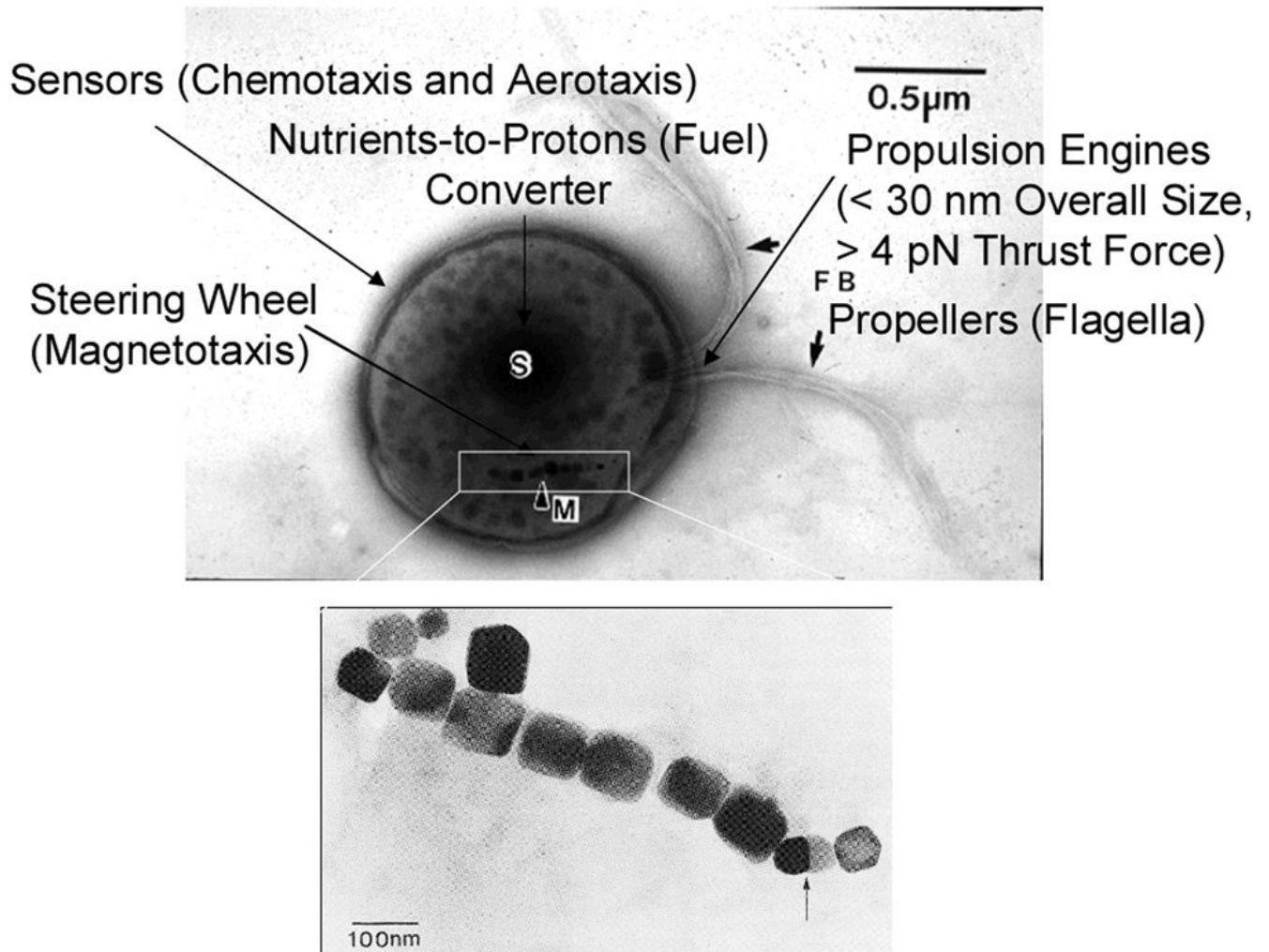


Fig. 1. Representation of the MC-1 MTB as a computer controllable bio-actuator with its flagella bundles (FB) for propulsion and its chain of magnetosomes (bottom) allowing steering control through magnetotaxis

MC-1 Velocity distribution at 20 Gauss

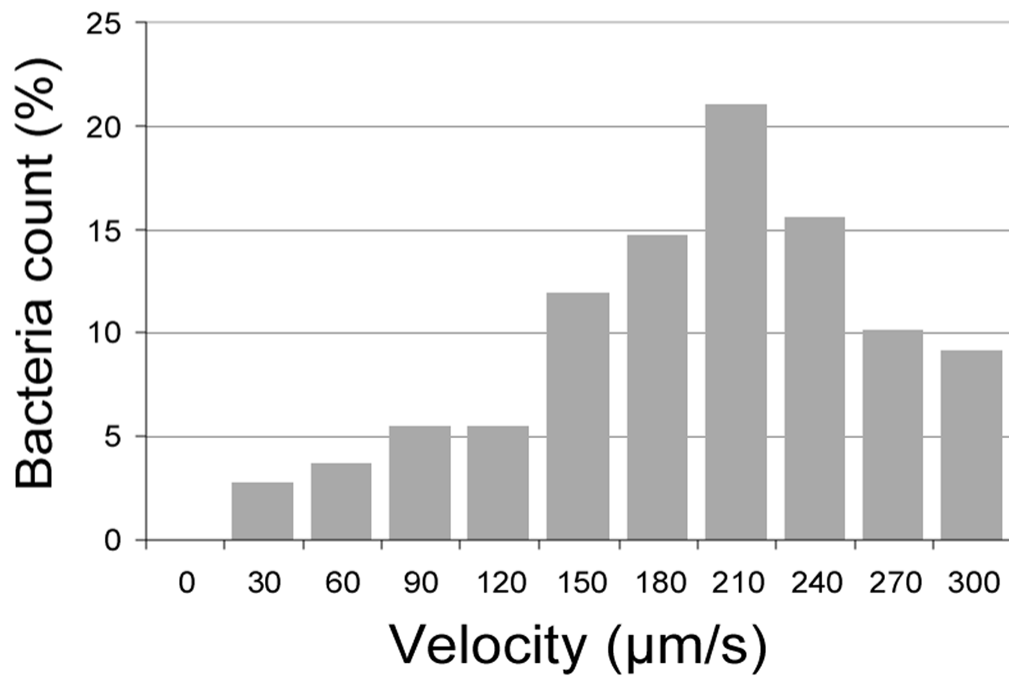


Fig. 2.
Swimming speed distribution of the unloaded and non pre-selected MC-1 bacteria in an aqueous medium at room temperature.

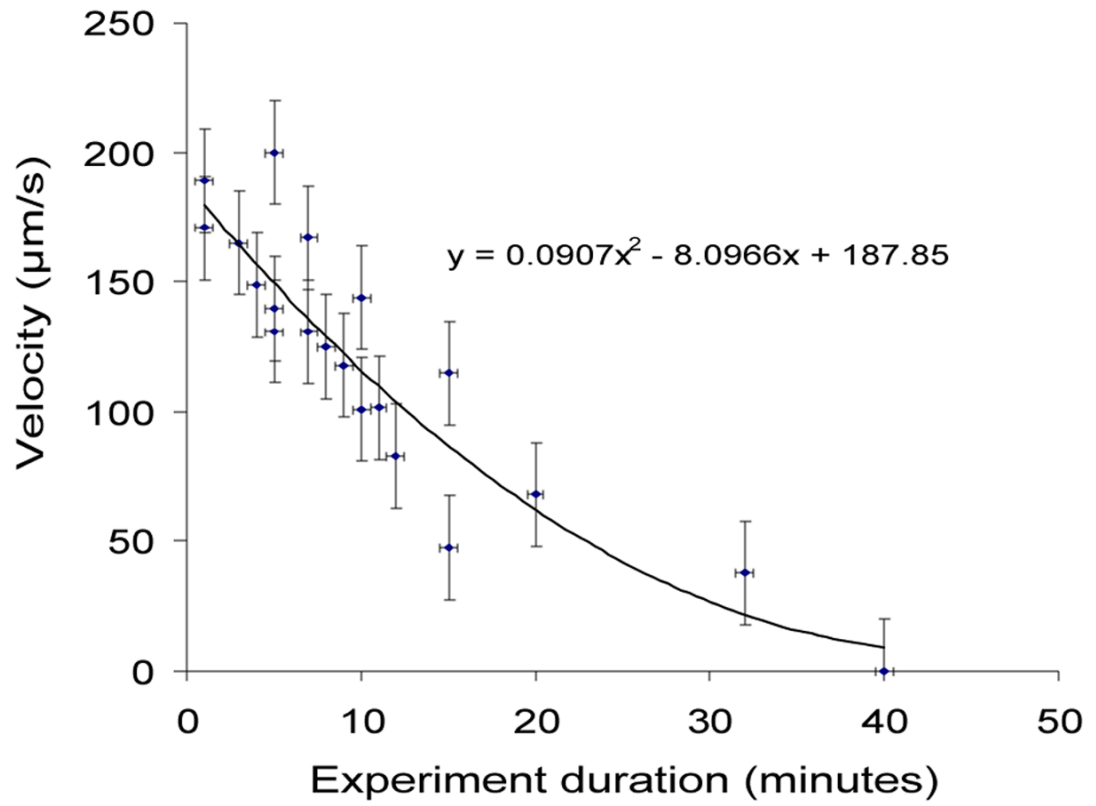


Fig. 3. Effect of the temperature on the swimming speed of unloaded MC-1 MTB in blood at 37°C

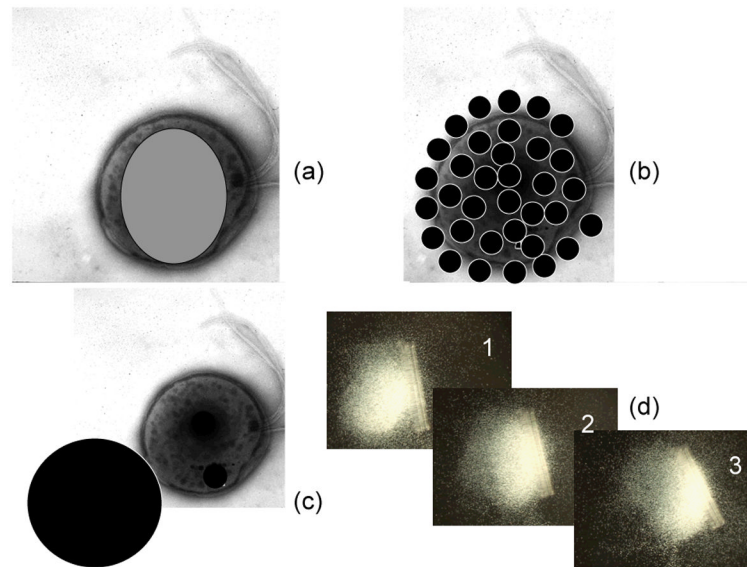


Fig. 4. Various loading strategies; (a) Loading inside the cell; (b) Attaching nanoparticles to the cell; (c) MTB pushing or pulling an attached microparticles or micro-objects such as demonstrated in (Martel et al. 2006); and (d) Experiments conducted by our research group showing a swarm of MTB used to move a larger object not attached to the MTB all under computer feedback control as seen by sequence 1 to 3 under an optical microscope.

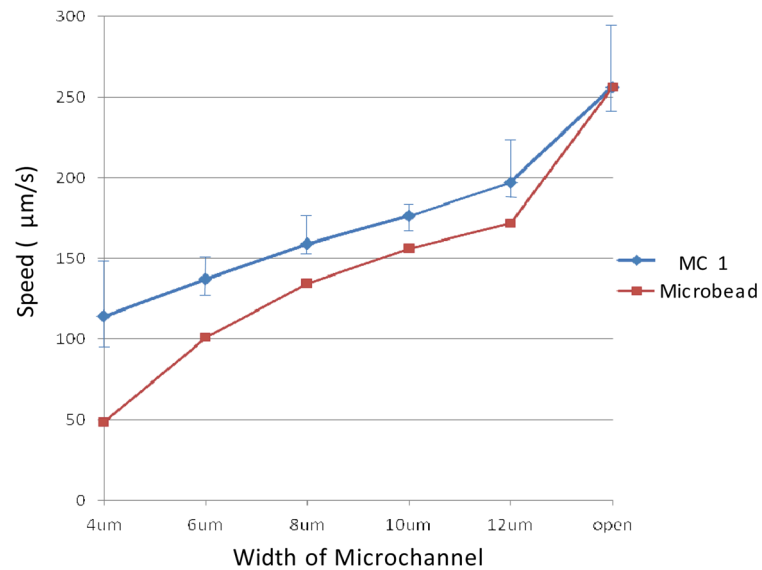


Fig. 5. Swimming speeds of the MC-1 cells (velocity of $223\mu\text{m/s}$ when not subject to wall effect) for different microchannel widths. The graph shows that the velocity in channel widths similar to the narrower capillaries decrease much less than the theoretical model applied to non-biological objects. Although this needs further investigation, this may suggest a thrust force compensation of the MC-1 bacteria when swimming in such conditions.

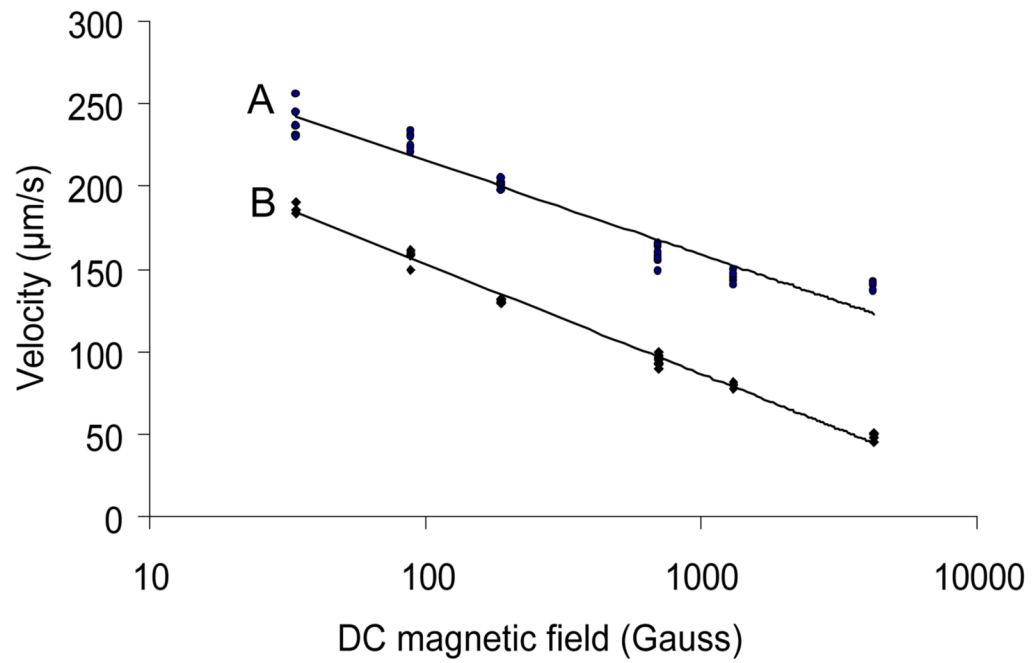


Fig. 6. Swimming speeds of the MC-1 bacteria versus the magnitudes of a Direct Current (DC) magnetic field. A: Bacteria have growth under anaerobic condition and only very small amounts of oxygen added daily. B: Bacteria have growth in medium containing 1% oxygen.

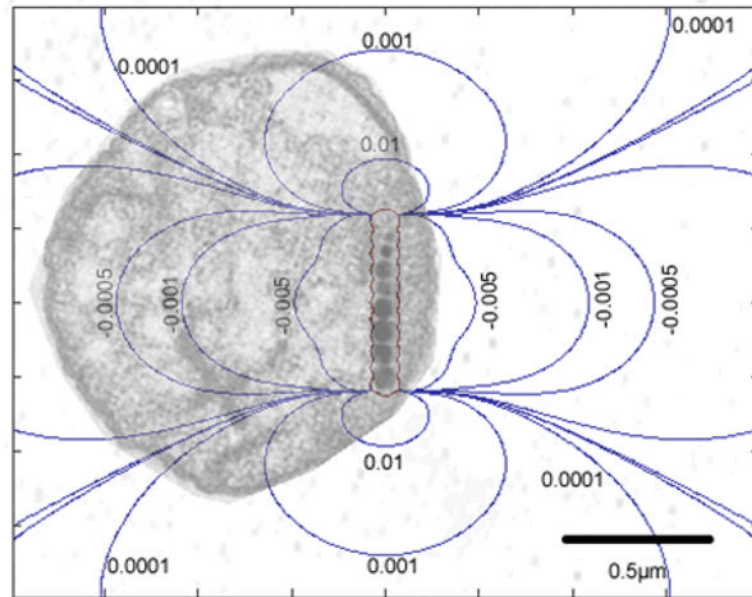


Fig. 7. Magnetic field lines (Tesla) generated by a magnetosome chain superimposed on an electron microscopy image of the bacterium. In this simulation, we consider the presence of 11 magnetosomes with a mean diameter of 70nm. The distance between the magnetosomes is of 20nm. The saturation magnetization for magnetite (0.6T) is considered since at the MRI field of 1.5T, the magnetite chain is saturated.

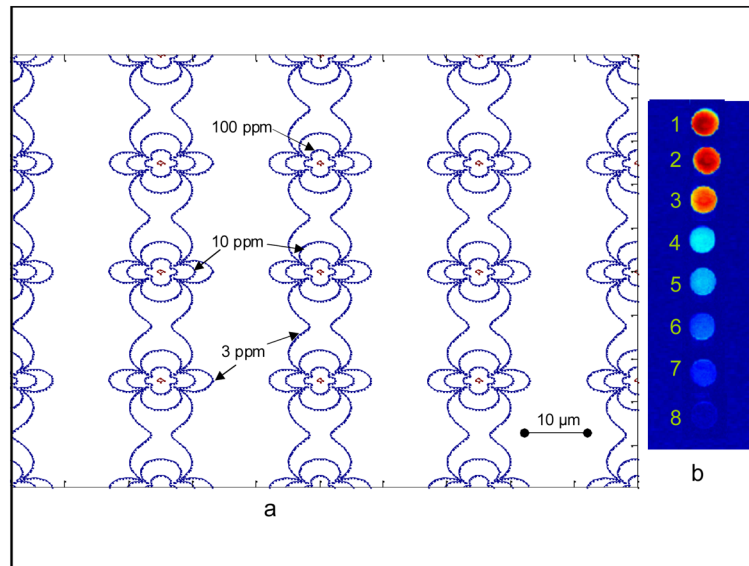


Fig. 8.

(a) Simulation of the local magnetic field perturbation for a uniformly distributed concentration of MTB; The distance between MTB is $25\mu\text{m}$ corresponding to a concentration of approximately 10^7 cells/ml. (b) Turbo spin echo sequence imaging of several samples of MTB of different concentrations. From 1 to 8 the concentrations are 0, 0.19, 0.30, 0.51, 0.73, 0.84, 0.90, 1×10^8 cells/ml. These experimental data confirm the possibility of tracking the MTB using MRI. The sequence parameters are TR/TE = 5620/127ms, Echo Train Length (ETL) = 27, 512×408 pixels and a spatial resolution of 0.254mm. When the concentration of MTB increases, the transverse relaxation rate increases leading to a decrease of the signal intensity.

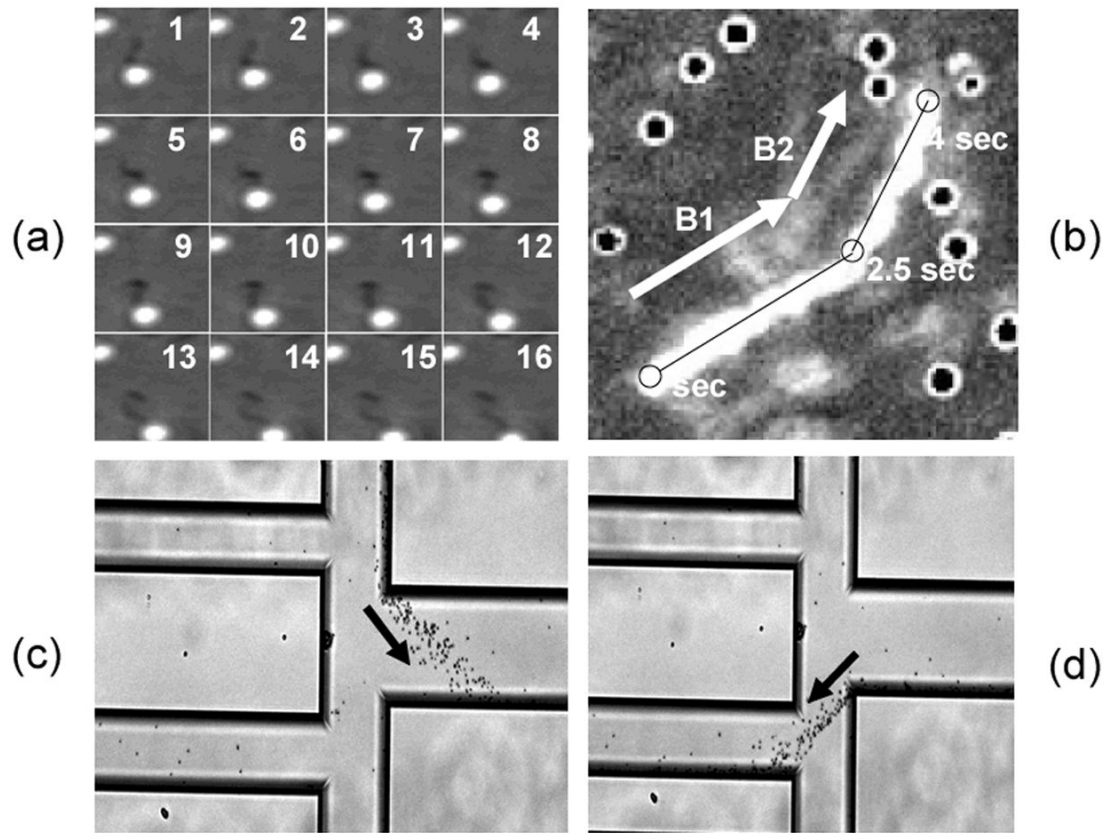


Fig. 9.

(a) A single MTB pushing a $3\mu\text{m}$ bead; (b) The same MTB pushing the bead and directed to turn left 30 degrees after 2.5 seconds, B1 and B2 indicate the direction of the magnetic field; (c) and (d) Swimming path of a swarm of MTB being controlled inside microfluidic channels.

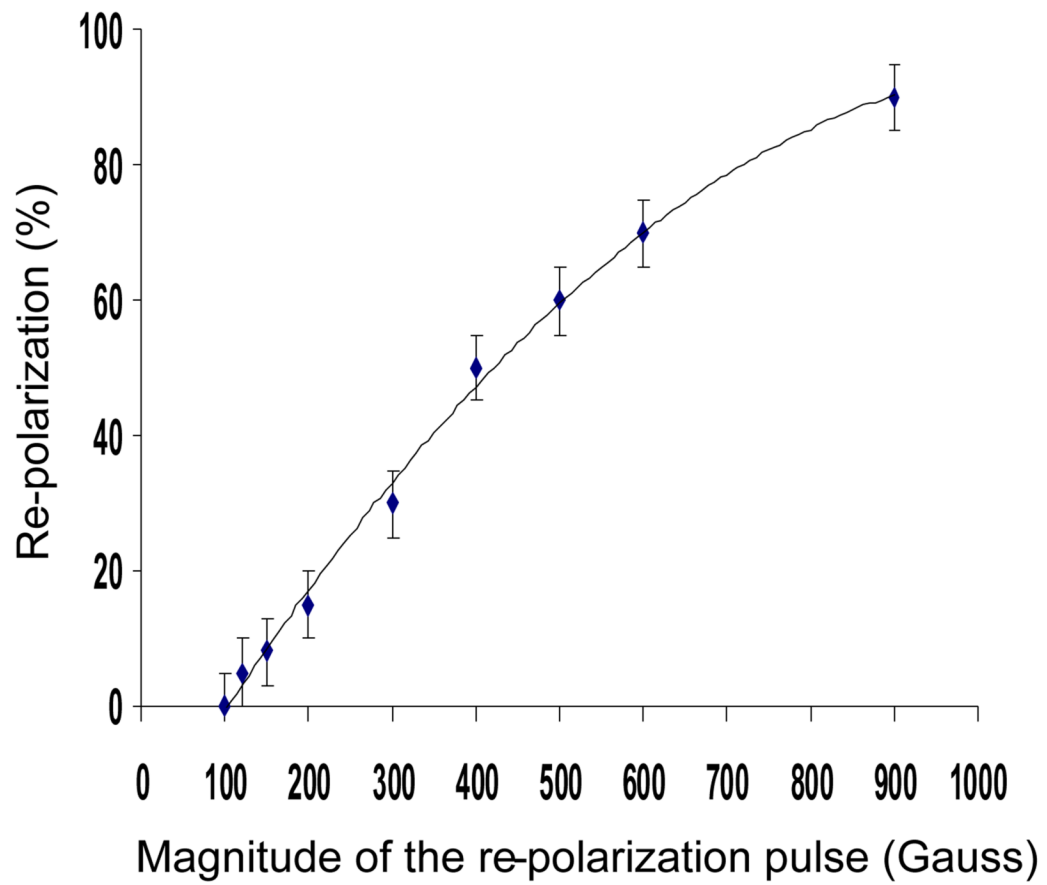


Fig. 10. Percentage of re-polarized (re-magnetized) MC-1 cells using a single one-second duration re-polarization pulse of different magnitudes

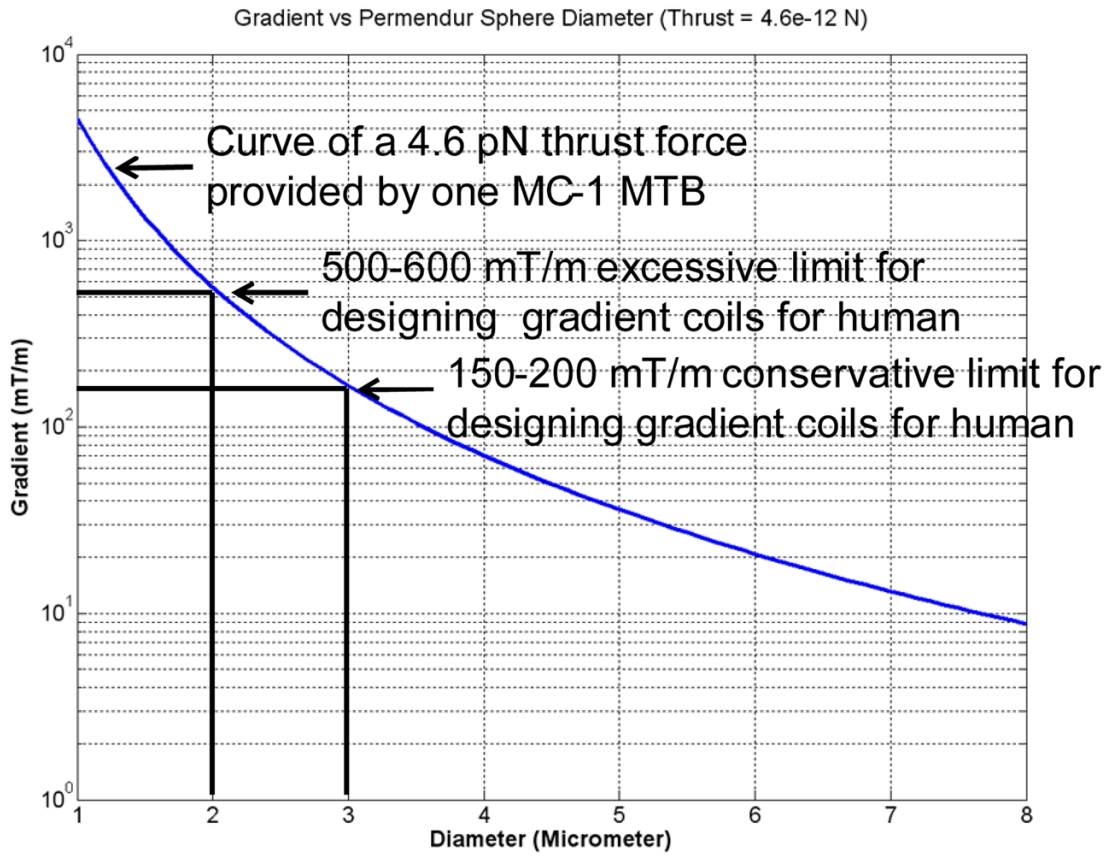


Fig. 11. MC-1 bacterium versus propulsion/steering magnetic gradient coils for human showing the potential advantage of bacterial actuation for carriers or nanorobots navigating in smaller capillaries. The graph considers 50% Permendur (highest magnetization saturation material) per unit volume to leave room for embedding therapeutic agents.

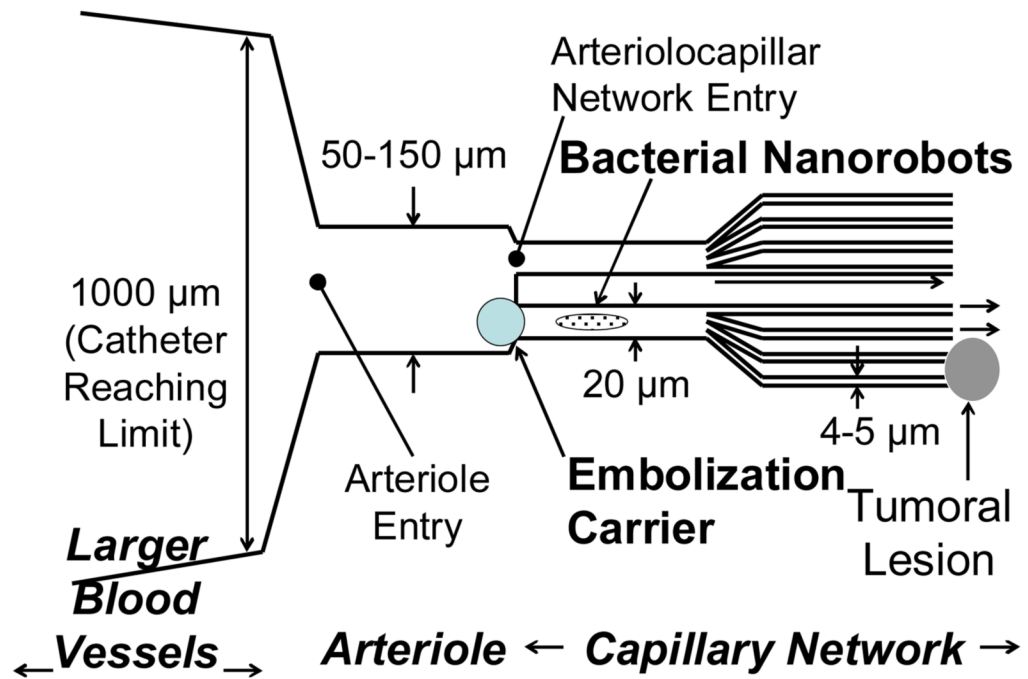


Fig. 12. Simplified schematics showing the various steps and vessel diameters used to reach the tumoral lesion.

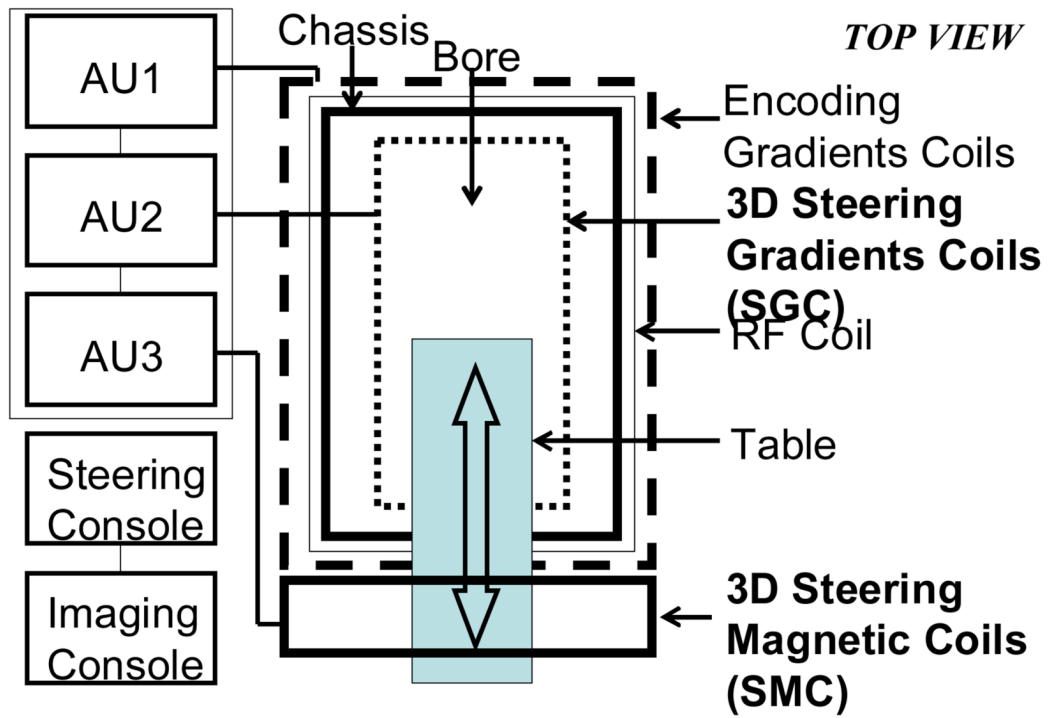


Fig. 13. Main hardware modules of the robotic platform for the MRI-trackable medical nanorobots

Appendix A

Index to Multimedia Extensions

| Extension | Type | Description |
|-----------|-------|---|
| 1 | Video | Directional control by computer of a swarm of MC-1 magnetotactic bacteria |